RSC Advances

Facile synthesis of nitrogen-doped unzipped carbon nanotubes and their electrochemical properties

Journal:	*RSC Advances*
Manuscript ID:	RA-ART-11-2014-015008.R1
Article Type:	Paper
Date Submitted by the Author:	22-Dec-2014

Complete List of Authors:	Chen, Liang; Hunan University, State Key Laboratory for Chemo/Biosensing and Chemometrics, College of Chemistry and Chemical Engineering Zhou, Haihui; Hunan University, State Key Laboratory for Chemo/Biosensing and Chemometrics, College of Chemistry and Chemical Engineering Wei, Shudan; Hunan University, State Key Laboratory for Chemo/Biosensing and Chemometrics, College of Chemistry and Chemical Engineering Chen, Zhongxue; Hunan University, State Key Laboratory for Chemo/Biosensing and Chemometrics, College of Chemistry and Chemical Engineering Huang, Zheng; Hunan University, State Key Laboratory for Chemo/Biosensing and Chemometrics, College of Chemistry and Chemical Engineering Huang, Zhongyuan; Hunan University, State Key Laboratory for Chemo/Biosensing and Chemometrics, College of Chemistry and Chemical Engineering Zhang, Chengping; Hunan University, State Key Laboratory for Chemo/Biosensing and Chemometrics, College of Chemistry and Chemical Engineering Kuang, Yafei; Hunan University,

Table of contents

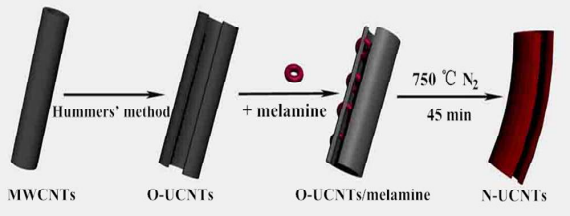

N-UCNTs with a high nitrogen level, large surface areas and good crystallinity are synthesized by pyrolysis of O-UCNTs/melamine composite.

Cite this: DOI: 10.1039/c0xx00000x

www.rsc.org/xxxxxx

ARTICLE TYPE

Facile synthesis of nitrogen-doped unzipped carbon nanotubes and their electrochemical properties

Liang Chen[a,b], Haihui Zhou[*a,b], Shudan Wei[a,b], Zhongxue Chen[a,b], Zheng Huang[a,b], Zhongyuan Huang[a,b], Chenping Zhang[a,b] and Yafei Kuang[*a,b]

Received (in XXX, XXX) Xth XXXXXXXXX 20XX, Accepted Xth XXXXXXXXX 20XX
DOI: 10.1039/c0xx00000x

In this work, a novel material based on nitrogen-doped unzipped carbon nanotubes (N-UCNTs) was synthesized by one step of pyrolysis of oxidized unzipped carbon nanotubes (O-UCNTs), which were prepared from pristine multiwalled carbon nanotubes (MWCNTs) according to the modified Hummers' method. Meanwhile, the supercapacitance and oxygen reduction reaction (ORR) behaviors of N-UCNTs were investigated in detail. The results demonstrate that, N-UCNTs show excellent performances in the application of supercapacitor and ORR, which can be attributed to the high nitrogen level (6.65 at.%), large surface area (215.8 m^2 g^{-1}) and good crystallinity of N-UCNTs. Therefore, it can be concluded that N-UCNTs provide a promising material candidate for the application in energy conversion and storage.

1. Induction

Carbon nanotubes (CNTs) as a special kind of carbon material have been studied extensively for a wide range of applications due to their unique fabric structure as well as excellent electrical and mechanical properties.[1-3] However, typical CNTs with lengths in the range of micrometers are easily aggregated into macroscopically entangled ropes or masses.[4-6] Meanwhile, for the structure of both ends closed, they often have relatively low surface areas, and the surface of CNTs is chemically inert, which limit their further development in the fields of energy conversion and energy storage (such as supercapacitor, oxygen reduction reaction and so on).[7-11]

Up to now, in order to overcome the structure deficiency of CNTs, considerable efforts have been devoted to the modification of CNTs.[12] The common methods of the modification of CNTs are chemical tailoring (including shortening and longitudinal tailoring)[13-18] and doping heteroatom (especially for N doping).[19-22] During the chemical tailoring of CNTs, for the intrusion of plentiful oxygen-containing groups on the surface of CNTs, the sp^2 structure of CNTs will be damaged to a certain degree, which leads to the loss of some excellent properties of CNTs.[23-24] Nevertheless, by chemically tailoring CNTs, it can greatly increase the surface areas of CNTs and avoid irreversible agglomeration to some extent. Moreover, it can bring in abundant oxygen-containing groups, which can act as reactive sites for further modification.[23-28] While doping the heteroatom into CNTs, the heteroatom will disrupt nanotube π-cloud, and have a profound effect on the structural arrangement and electronic properties of CNTs, which makes heteroatom-doped CNTs excellent candidates for a new generation of controlled chemically functionalised materials.[29-32] The common approaches to doping the heteroatom into CNTs can be categorized into two ways[30,33]: (i) doping heteroatom directly during the synthesis of CNTs, which can be called as "in situ" doping; (ii) post-treatment of presynthesized CNTs with different nitrogen sources, i.e., post-doping. Generally, the "in situ" doping methods, such as arc-discharge, laser ablation or chemical vapor deposition (CVD), perform under a strict condition and use very expensive apparatus.[34-37] When using the post-doping method, the doped CNTs always exhibit a low doping level, which can be ascribed to the structure deficiency of CNTs. Specifically, the lack of the reactive doping sites on the surface of CNTs leads to a low doping level of the doped CNTs.[33,38]

Generally, it is reported that CNTs regarded as closed-curly graphene, can be longitudinally tailored into unzipped CNTs (UCNTs) by the chemical oxidation method. During the process of longitudinal tailoring, a lot of oxygen-containing functional groups (such as hydroxyls, carboxyls etc.) are brought onto the surface of CNTs, which leads to the formation of the highly oxidized unzipped carbon nanotubes (O-UCNTs).[14,17,18,25] Compared to pristine CNTs, the O-UCNTs with a lot of oxygen-containing functional groups not only show larger surface areas, but also avoid irreversible agglomeration to some extent for their unzipped structure. More significantly, the oxygen-containing functional groups on the surface of O-UCNTs can act as the

[a] *State Key Laboratory for Chemo/Biosensing and Chemometrics, Hunan University, Changsha, China; Fax: +86-731-88713642; Tel:+86-731-88821603;*
[b] *College of Chemistry and Chemical Engineering, Hunan University, Changsha, China; Fax: +86-731-88713642; Tel:+86-731-88821603; E-mail: yafeik@163.com(Yafei Kuang), haihuizh@163.com(Haihui Zhou)*

reactive sites for the further modification, which observably broadens the application of CNTs in the fields of energy conversion and energy storage.

In our work, chemical tailoring and nitrogen doping of CNTs are achieved together and the nitrogen-doped unzipped carbon nanotubes are successfully synthesized. At the beginning, the O-UCNTs with a lot of oxygen-containing groups are prepared from pristine multiwalled carbon nanotubes (MWCNTs) according to the modified Hummers' method. And then by adding the low-cost industrial material melamine as the nitrogen source, a homogenous O-UCNTs/melamine composite is obtained for the strong interaction between O-UCNTs and melamine. After that, the simultaneous N doping and reduction of the O-UCNTs can be achieved just by one step of pyrolysis at 750 °C for 45 minutes under a N_2 atmosphere. As a consequence, the N-UCNTs with a high nitrogen level, large surface areas and good crystallinity can be synthesized for a large scale. Considering the wide use of nitrogen-doped carbon materials in the fields of supercapacitor and oxygen reduction reaction (ORR),[21,28,30,36,38] the supercapacitance and ORR behaviors of N-UCNTs are investigated in detail.

2. Experimental

2.1. Chemicals and materials

All reagents (Sinopharm Chemical Reagent Co., Ltd., China) were of analytical grade without further treatment. Ultrapure water was used in this study. The pristine multi-walled carbon nanotubes (MWCNTs, purity>97%) with 5-15 μm in length and 60-100 nm in diameter were commercially supplied (L-MWNT-60100, Shenzhen Nanotech Port Co., Ltd.).

2.2. Preparation of O-UCNTs

In a typical synthesis, O-UCNTs were prepared from the pristine MWCNTs by using the modified Hummers' method.[11,41] Briefly, 1 g of MWCNTs and 0.5 g of sodium nitrate were dispersed in 46 mL of concentrated sulfuric acid (98%) in a 250 mL roundflask. The mixture was stirred in an ice bath for about 0.5 h. And then 5 g of potassium permanganate was slowly added into the suspension under vigorous stirring. After that, the resulting mixture was removed from the ice bath and then stirred at 40 °C for 2.5 h. Next, 50 mL of water was gradually added with vigorous agitation. After the solution cooled to room temperature, 5 mL of H_2O_2 (30 wt.%) and 100 mL of water were separately added. The final obtained mixture was centrifuged and washed with ethanol and deionized water for several times until the pH of the suspension was close to 7. The final products were dried at 60 °C under vacuum for 24 h as a result of O-UCNTs.

2.3. Preparation of N-UCNTs, N-CNTs and UCNTs

N-UCNTs were produced by a method similar to the previous reports.[42-44] O-UCNTs were dispersed in deionized water (0.5 g/L) by ultrasonication. Then, melamine was added to O-UCNTs (2.5 g/L) and stirred overnight. The resulting dispersion was dried at 80 °C in an oven and the solid material was grinded into fine powders by using a mortar. The obtained composite was pyrolysed at 750 °C for 45 minutes under a N_2 atmosphere to prepare N-UCNTs. In contrast, N-CNTs were produced via the same doping method just by substituting the O-UCNTs with pure CNTs. At the same time, the unzipped carbon nanotubes (UCNTs) were synthesized by using the similar pyrolysis method without the addition of melamine.

2.4. Characterization

The microstructure of the as-prepared sample was observed by scanning electron microscope (SEM) (Hitachi S-4800, Japan) and transmission electron microscope (TEM) (JEM-2100F, Japan). Thermogravimetric analysis (TGA) was carried out on a simultaneous DSC-TGA analyzer (NETZSCH-409PC). Samples were heated from room temperature to 800 °C with a heating rate of 10 °C min^{-1} under a continuous flow of nitrogen gas. Fourier transform infrared spectra (FTIR) characterization was performed at ambient temperature with a NICOLET 6700 FTIR spectrometer. X-ray photoelectron spectroscopy (XPS) analysis was conducted on ESCALAB250 XPS spectrometer with an Mg Kα X-ray source (1350 eV). Specific surface area and pore size distribution were calculated based on the nitrogen physical sorption (Beckman Coulter SA-3100, USA). The X-ray diffraction (XRD) patterns were examined by using an X-ray diffractometer (XRD, Philips PC-APD) with Cu Kα radiation (λ= 1.5418 Å) operating at 40 kV, 60 mA.

2.5. Electrochemical measurements

The capacitive performance tests were conducted using 6 M KOH electrolyte in a conventional three-electrode cell on a CHI 660C electrochemical workstation (Shanghai Chenhua Instrument, China). A platinum foil electrode and saturated calomel electrode (SCE) were used as the auxiliary and reference electrodes, respectively. The working electrode was prepared by dropping 0.5 mg mL^{-1} of well-dispersed electrode material solution (50 μL) onto a glassy carbon electrode with a diameter of 5 mm. The capacitive performances of electrodes were measured using cyclic voltammetry (CV) and electrochemical impedance spectroscopy (EIS). CV tests were measured at different scan rates within a voltage range from 0.1 V to -0.8 V (*vs.*SCE) and EIS measurements were operated on open circuit potential at the frequency range of 0.01 Hz-100 kHz.

The ORR performance tests were carried out using 0.1 M KOH electrolyte in a conventional three-electrode cell on the CHI 660C electrochemical workstation. A platinum foil electrode and a Ag/AgCl electrode filled with saturated KCl aqueous solution were used as the auxiliary and reference electrodes, respectively. The electrocatalytic activities towards ORR were measured using a rotating disk electrode (Pine Instrument, MSR analytical rotator). 20 μL of 1 mg mL^{-1} well-dispersed electrode material solution was transferred onto a pre-polished glassy carbon electrode (5 mm diameter). After drying at room temperature, the electrode was covered with 5 μL of 0.05 wt% Nafion solution and then was put under vacuum for 30 min before measurement. 0.1 M KOH solution was prepared as the electrolyte and saturated with oxygen by bubbling with oxygen gas at least for an hour. The linear sweep voltammetry (LSV) at a

scan rate of 10 mV s^{-1} was performed at various rotation speeds from 400 to 1600 rpm.

3. Results and discussion

The synthesis of N-UCNTs involves three steps, and a schematic illustration is shown in **Fig.1**. At the beginning, the pristine MWCNTs were split to prepare the O-UCNTs according to the modified Hummers' method. Subsequently, an appropriate amount of melamine was added into the O-UCNTs solution. After the O-UCNTs/melamine composite was obtained by drying the mixed solution in an oven at 80 ℃ overnight, the obtained solid powder was pyrolysed at 750 ℃ for 45 minutes under a N_2 atmosphere to prepare the N-UCNTs.

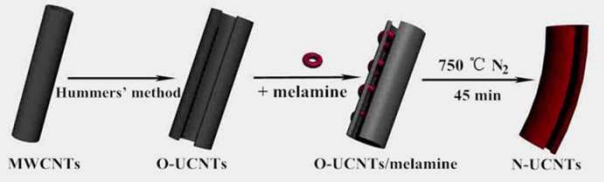

Fig.1 Schematic diagram of the synthesis of N-UCNTs

Fig.2a and **Fig.2b** show the SEM images of pristine MWCNTs and O-UCNTs, respectively. As shown in **Fig.2b**, the unzipped structure of O-UCNTs is clearly observed, and the irreversible agglomeration is avoided to some extent when compared to pristine MWCNTs. **Fig.2c** shows the SEM image of N-UCNTs. Obviously, the wrinkled morphology of N-UCNTs can be clearly observed, which can be ascribed to the nitrogen doping of MWCNTs. And the width of N-UCNTs increases to more than 150 nm, which can be attributed to the successful chemical tailoring. The unzipped structure of N-UCNTs can be clearly seen from the red arrow area in **Fig.2c**. **Fig.2d** shows the HRTEM of N-UCNTs. According to **Fig.2d**, the interlayer spacing of N-UCNTs is calculated as 3.36 Å, which is close to the ideal graphite interlayer spacing (3.34 Å).

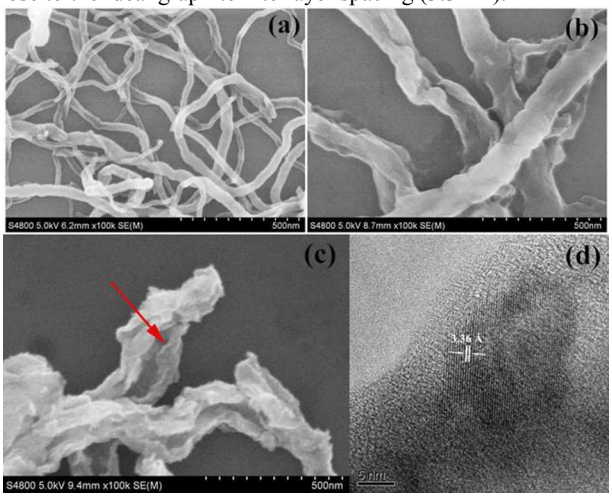

Fig.2 SEM images of MWCNTs (a), O-UCNTs (b), N-UCNTs (c) and HRTEM (d) image of N-UCNTs

Fig.S1 (ESI) shows TGA curves of MWCNTs and O-UCNTs, respectively. As clearly revealed from **Fig.S1**, there is almost no weight loss when MWCNTs are heated from room temperature to 800 ℃ under nitrogen atmosphere, while there is a significant weight loss about 40% under the same condition for O-UCNTs, which indicates the existence of a large number of labile O-containing groups in O-UCNTs. In order to further demonstrate the existence of a lot of O-containing groups in O-UCNTs, the chemical structure of O-UCNTs was investigated using FTIR, as shown in **Fig.S2** (ESI). In the spectrum of O-UCNTs, an obvious peak at ~3400 cm^{-1}, a signature for -OH groups, indicates that the hydroxyl group is one of the residual O-containing groups in O-UCNTs. The three peaks at ~1720 cm^{-1}, ~1630 cm^{-1} and 1240 cm^{-1} can be ascribed to the C=O in COOH, aromatic C=C and C-OH, respectively. By contrast, as shown in the FTIR spectrum of MWCNTs, the weak peak at ~3300 cm^{-1} which can be attributed to the -OH groups shows that MWCNTs are oxidized to some extent. As to MWCNTs, the relative intensity of the peak at ~3300 cm^{-1} is weaker than that of O-UCNTs, which shows that the amount of the O-containing functional groups of O-UCNTs is much larger than those of MWCNTs.

According to the results of TGA and FTIR, it can be concluded that O-UCNTs are a highly oxidized carbon-based material with many O-containing moieties, such as hydroxyls, epoxies, carbonyls and carboxyls, which makes them hydrophilic and brings in negative charges on the surface. After adding melamine, the nature of O-UCNTs/melamine interaction could be ionic bonding between protonated amines and carboxyls, hydrogen bonding between the amine group in melamine and O-containing groups in O-UCNTs, or π-π interaction between unoxidized area in O-UCNTs and triazine rings.[42-43] The strong interaction between O-UCNTs and melamine makes a homogenous O-UCNTs/melamine composite. At this moment, the local areas with lots of O-containing groups on the surface of O-UCNTs can play the role of reactive doping sites. As a result, an effective doping method is expected in the field of the synthesis of N-doped carbon materials.

To demonstrate the successful nitrogen doping in N-UCNTs, the XPS spectra of N-UCNTs and N-CNTs were investigated in detail, which was evidently presented in **Fig.3**.

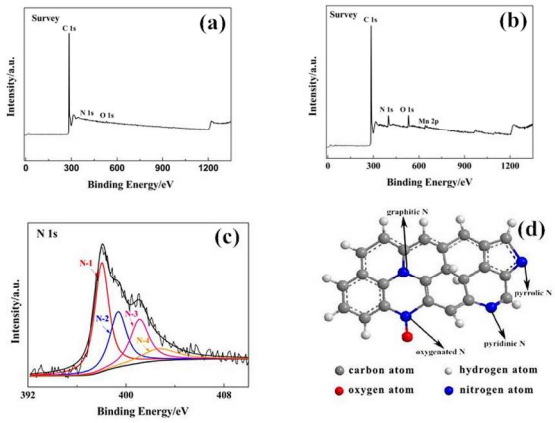

Fig.3 XPS survey of N-CNTs (a), N-UCNTs (b), high resolution N 1s

spectra of N-UCNTs (c) and schematic diagram of four different kinds of N (d). N 1s peak is deconvoluted into four sub-peaks that correspond to pyridinic N (N-1), pyrrolic N (N-2), graphitic N (N-3), and oxygenated N (N-4)

According to **Fig.3a**, the XPS spectrum of the N-UCNTs shows the presence of C 1s, O 1s, N 1s and Mn 2p. In the meantime, the XPS spectrum of the N-CNTs also shows the existence of C 1s, O 1s, N 1s, which is clearly shown in **Fig.3b**. And the specific XPS results are displayed in **Table 1**.

Table 1 XPS results of N-CNTs and N-UCNTs

	XPS [at.%]			
Samples	C	O	N	Mn
N-CNTs	98.22	1.32	0.46	-
N-UCNTs	86.86	6.01	6.65	0.48

Obviously, the N-UCNTs of high nitrogen content (6.65 at.%) is triumphantly obtained when compared to N-CNTs (0.46 at.%). The oxygen content (6.01 at.%) of N-UCNTs mainly arises from the thermally stable O-containing groups on the surface of N-UCNTs. Meanwhile, the existence of a tiny amount of Mn (0.48 at.%) can be attributed to the introduction of $KMnO_4$ during the preparation of O-UCNTs. During the pyrolysis of O-UCNTs/melamine composite, the form of amino N which exists in melamine will disappear, which was reported in previous study.[42] Thus only four different kinds of N, pyridinic N (N-1), pyrolic N (N-2), graphitic N or quaternary N (N-3) and oxygenated N (N-4) may exist in N-UCNTs. As revealed from **Fig.3c**, the N 1s spectra can be fitted by four peaks located at 398.1, 399.6, 401.2 and 403.0 eV, representing N-1, N-2, N-3, and N-4, respectively.[42,45,46] As shown in **Fig.3d**, the schematic diagram of the four different kinds of N is presented. The N-1 (48.51%) is incorporated by substituting a carbon atom on a C_6 ring, which provides one pair of lone electrons. The N-2 (29.09%) refers to the N atom contributing two p-electrons to the π system. N-2, which is not present in precursor melamine, is probably a product of the reaction between O-UCNTs and amino groups in melamine. The N-3 atoms, doped inside the graphitic carbon plane, are bonded with three sp^2 carbon atoms, generating a positive charge and electron-acceptor properties. The percentage of N-3 is up to 16.67%, which can be attributed to the structural similarity between melamine and N-UCNTs.[47]

Fig.4 presents the N_2 adsorption/desorption isotherm curve of N-UCNTs. Obviously, the as-prepared N-UCNTs exhibits type IV characteristic, which suggests the mesoporous characteristic of N-UCNTs. Zhang et. al [11] reported that the pristine MWCNTs have the specific surface area and pore volume of 83.09 $m^2\ g^{-1}$ and 0.013 $cm^3\ g^{-1}$, respectively. When compared to the pristine MWCNTs, the specific surface area and pore volume of N-UCNTs dramatically increase to 215.8 $m^2\ g^{-1}$ and 0.171 $cm^3\ g^{-1}$, respectively. At the same time, N-UCNTs show an average pore size of 3.180 nm. It is apparent that the large specific surface area and pore volume of N-UCNTs can be mostly attributed to the longitudinal tailoring of pristine MWCNTs.

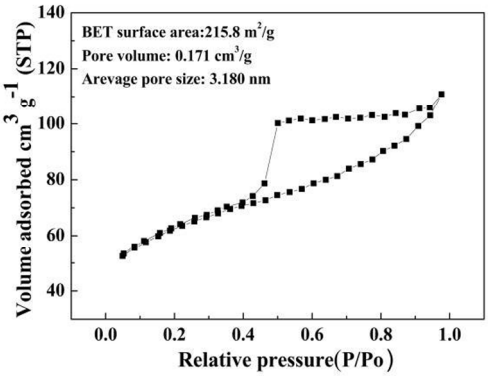

Fig.4 Nitrogen adsorption/desorption isotherm curve of N-UCNTs

Fig.5 exhibits the wide-angle powder XRD patterns of MWCNTs, O-UCNTs and N-UCNTs. As shown in **Fig.5**, the XRD pattern of MWCNTs shows a sharp peak at 2θ=26.2°. After the longitudinal split of MWCNTs, the sharp 002 diffraction peak disappears while a new peak of O-UCNTs appears at 2θ=9.2°, which implies that abundant O-containing groups exist on the surface of O-UCNTs. After the pyrolysis of O-UCNTs/melamine composites, it's clear that the 002 peak of N-UCNTs appears at 2θ=26.5°, and the disappearance of the relatively broad peak at around 9.2° confirms the reduction of O-UCNTs. As is known to us, the crystallinity of carbon-based materials has intimate relation with their interlayer spacing. And the interlayer spacing (d_{002}) decreases as the crystallinity of a sample improves.[47-48] According to the Bragg equation, the values of d_{002} of MWCNTs, O-UCNTs and N-UCNTs are 3.40 Å, 9.61 Å and 3.36 Å, respectively, which is accorded with the result of HRTEM. The decrease of the value of d_{002} demonstrates the good crystallinity of N-UCNTs, which may be ascribed to the successful nitrogen-doping of N-UCNTs.[48]

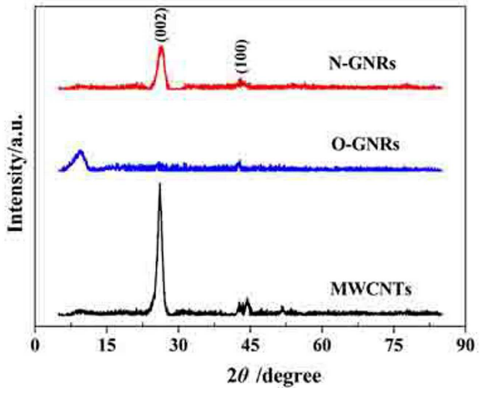

Fig.5 XRD patterns of MWCNTs,O-UCNTs and N-UCNTs

Based on the morphology and structure analysis, N-UCNTs are expected to exhibit excellent electrochemical properties in the application of supercapacitor and ORR. **Fig.6** shows the CV curves of UCNTs and N-UCNTs at the scan rate of 50 mV s^{-1} in 6 M KOH electrolyte. The CV curve of N-UCNTs shows a

unique quasirectangular shape, and the appearance of a couple of less clear redox peaks at -0.36 V and -0.60 V can be attributed to the pseudocapacitive contribution from redox reactions of the functional groups on the surface of the electrodes. It is obvious that the loop area of N-UCNTs is larger than that of UCNTs, which mainly results from the pseudocapacitance caused by N doping.[49-51]

The specific capacitance of N-UCNTs at different scan rates can be calculated according to the following equation:

$$C = \frac{\oint_{Va}^{Vb} I(V)dV}{2mv(V_a - V_b)}$$

Where C is the specific capacitance (F g^{-1}), m is the mass of the electrode active materials (g), v is the scan rate of CV curves (V s^{-1}), (V_a–V_b) represents the potential window (V). The specific capacitance of N-UCNTs (221 F g^{-1}) is almost twice larger than that of UCNTs (115 F g^{-1}) at the scan rate of 50 mV s^{-1}.

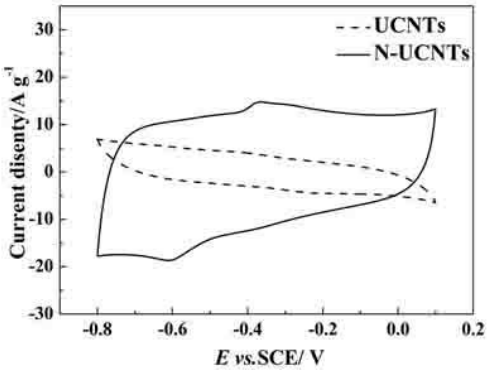

Fig.6 CV curves of UCNTs and N-UCNTs at the scan rate of 50 mV s^{-1} in 6 M KOH electrolyte

Rate capability is another crucial criterion for estimating the practical application of electrode materials used in supercapacitors. **Fig.S3** (ESI) shows the CV curves of N-UCNTs electrode with various scan rates from 5 to 100 mV s^{-1} in 6 M KOH electrolyte. All the CV curves of N-UCNTs show quasi-rectangular shape, even at a high scan rate of 100 mV s^{-1}, which indicates that N-UCNTs, as supecapacitor electrode materials, have a good rate capacitive behavior and a low contact resistance. **Fig.S4** (ESI) shows the EIS of UCNTs and N-UCNTs, respectively. Clearly, the slope of the plot for N-UCNTs is steeper than that for UCNTs, affirming that better capacitive behaviour is a characteristic of N-UCNTs.[52] Meanwhile, N-UCNTs exhibit a smaller semicircle when compared to UCNTs. This indicates that N-UCNTs have a lower charge-transfer resistance[53] and more excellent conductivity due to the good crystallinity and high nitrogen content of N-CNTs.[47,54] **Fig.S5** (ESI) shows the cyclic stability of N-UCNTs in 6 M KOH electrolyte at the constant scan rate of 100 mV s^{-1}. It is clear that the specific capacitance of N-UCNTs maintains over 90% of the initial specific capacitance after 10000 consecutive cycles. Therefore, N-UCNTs show high specific capacitance, good rate capability and good cycling stability in application of supercapacitor.

Rotating disk electrode (RDE) technique is used to investigate the electrocatalytic activity of N-UCNTs towards ORR by LSV.[21] As shown in **Fig.7**, the reduction of oxygen on N-CNTs shows a two-step two electron process with the formation of intermediate HO_2^- ions as indicated by two reduction waves starting at -0.22 V and -0.60 V, respectively. By contrast, the oxygen reduction reaction on N-UCNTs sample starts at -0.08 V. Obviously, the onset potential of N-UCNTs is more positive than that of N-CNTs and the reduction current of N-UCNTs is also much larger than that of N-CNTs. This demonstrates that N-UCNTs have a better electrocatalytic activity towards ORR than N-CNTs. The electrocatalytic activity of N-UCNTs towards ORR is also more superior to the nitrogen-doped graphene that was synthesized using the method,[42] which may be attributed to the high N content of N-UCNTs (especially for the graphitic N and pyridinic N, graphitic N content determines the limiting current density and the pyridinic N content improves the onset potential for ORR).[55-56]

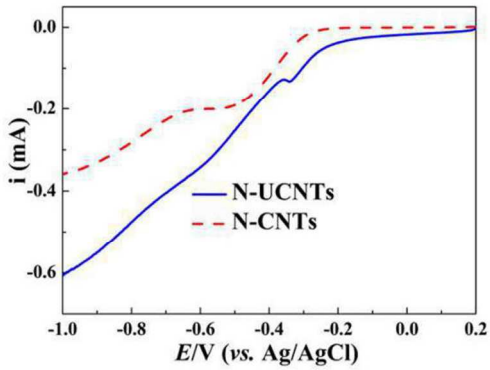

Fig.7 Linear sweep voltammetric curves (LSVs) of ORR on N-CNTs and N-UCNTs disk electrode in O_2-saturated 0.1 M KOH electrolyte (scan rate: 10 mV s^{-1}, rotation speed: 1600 rpm)

In order to understand the catalytic mechanism, LSV curves of RDE loaded with N-UCNTs sample were recorded at various rotation speeds, as shown in **Fig.8**. The reduction current increases with increasing rotation speed for N-UCNTs, as shown in **Fig.8a**. The transferred electron number per oxygen molecule in the ORR process was calculated by the Koutechy-Levich (K-L) equation $(i^{-1}=i_k^{-1}+i_L^{-1}=(nFAkC_0)^{-1}+(0.62nFAD^{2/3}C_0v^{-1/6}\omega^{-1/2})^{-1})$, where, i is the measured current, i_k and i_L are the kinetic- and limiting- currents, respectively. n is the electron transfer number in the ORR process, F is the Faraday constant (96485 C mol^{-1}), A is the geometric area of RDE, D is the diffusion coefficient of O_2 in the KOH electrolyte (1.9×10^{-5} cm^2 s^{-1}), C_0 is the bulk concentration of O_2 (1.2×10^{-3} M), v is the kinetic viscosity of the electrolyte (0.01 cm^2 s^{-1}), ω is the angular velocity of the disk ($\omega=2\pi N$, N is the linear rotation speed) and k is the electron transfer rate constant. **Fig.8b** showed the plots of i^{-1} vs. $\omega^{-1/2}$ for N-UCNTs. The average electron transfer number n for ORR was calculated as 3.38 at the potential of -0.80 V, suggesting a close

four-electron transfer ORR occurs on the N-UCNTs. Thus, according to the LSV results, it can be deduced that N-UCNTs exhibit huge potential in the aspect of ORR.

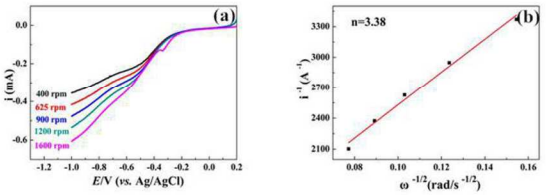

Fig.8 (a) RDE voltammograms for the ORR on the N-UCNTs electrode at various rotation speeds (scan rate: 10mV s^{-1}); (b) Koutechy-Levich plot (i^{-1} versus $\omega^{-1/2}$) at the potential of -0.80 V

4. Conclusions

In summary, a novel nitrogen-doped unzipped carbon nanotubes (N-UCNTs) were triumphantly synthesized in our work. By chemically tailoring the pristine CNTs, the O-UCNTs with large surface areas can be obtained. Meanwhile, it can bring in lots of reactive doping sites for nitrogen doping on the surface of O-UCNTs. When the obtained O-UCNTs/melamine composite is pyrolysed under a N_2 atmosphere, the successful N doping and reduction of the O-UCNTs can be achieved at the same time. As a result, the N-UCNTs were obtained. The as-prepared N-UCNTs exhibit a high nitrogen level (6.65 at.%), large surface area (215.8 m^2 g^{-1}) and good crystallinity. These features provide the N-UCNTs with excellent performances in the application of supercapacitor and ORR, that is, with high specific capacitance, good rate capability, good cycling stability for supercapacitor and a high electrocatalytic activity for ORR.[47,55,56] Thus, it can be deduced that N-UCNTs provide a promising material candidate for the application in energy conversion and storage.

5. Acknowledgements

This work was supported by National Natural Science Foundation of China (Grant No.51071067, 21271069, J1210040, 51238002) and Science and Technology Program of Hunan Province.

Notes and References

1 S. Frank, P. Poncharal, Z. L. Wang, W. A. de Heer, *Science*, 1998, 280, 1744–1746.
2 W. Liang, M. Bockrath, D. Bozovic, J. H. Hafner, M. Tinkham, H. Park, *Nature*, 2001, 411, 665–669.
3 E. W. Wong, P. E. Sheehan, C. M. Lieber, *Science*, 1997, 277, 1971–1975.
4 Kirk J. Ziegler , Zhenning Gu , Haiqing Peng ,Erica L. Flor , Robert H. Hauge, Richard E. Smalley, *J. Am. Chem. Soc.*, 2005, 127, 1541-1547.
5 X. X. Wang, J. N. Wang, L. F. Su, J. J. Niu, *J. Mater. Chem.* , 2006, 16, 4231-4234.
6 K. J. Ziegler, Z. N. Gu, J. Shaver, Z. Y. Chen, E. L. Flor, D. J. Schmidt, C. Chan, R. H. Hauge, R. E. Smalley, *Nanotechnology*, 2005, 16, S539-S544.
7 S. Wang, Z. Y. Liang, B. Wang, C. Zhang, Z. Rahman, *Nanotechnology*, 2007, 18, 055301.
8 P. M. Ajayan , T. W. Ebbesen , T. Ichihashi , S. Iijima, K. Tanigaki, H. Hiura, *Nature*, 1993, 362, 522-525.
9 S. C. Tsang, Y. K. Chen, P. J. F. Harris, M. L. H. Green, *Nature*, 1994, 372, 159- 162.
10 Y. S. Yun, H. H. Park, H. J. Jin, *Material*, 2012, 5, 1258-1266.
11 C. J. Zhang, H. H. Zhou, X. Q. Yu, D. Shan, T. T. Ye, Z. Y. Huang, Y. F. Kuang, *RSC Adv.*, 2014, 4, 11197-11205.
12 R. H. Baughman, A. A. Zakhidov , W. A. de Heer, *Science*, 2002, 297, 787-792.
13 D. V. Kosynkin, A. L Higginbotham, A. Sinitskii, J. R. Lomeda, A. Dimiev, B. K. Price, J. M. Tour, *Nature*, 2009, 458, 872-876.
14 Y. L. Liao, Z. F. Chen, J. W. Connell, C. C. Fay, C. Park, J. W. Kim, Y. Li, Adv. Funct. Mater., 2014, 4497-4506.
15 Y. Wei, P. Liu, F. Zhu, K. L. Jiang, Q. Q. Li, S. S. Fan, *Nano Lett.*, 2012, 12, 2071-2076.
16 S. H. Lee, D. H. Lee, W. J. Lee, S. O. Kim, Adv. Funct. Mater., 2011, 21, 1338-1354.
17 L. M. Xie , H. L. Wang , C. H. Jin, X. R. Wang, L. Y. Jiao, K. Suenaga, H. J. Dai, *J. Am. Chem. Soc.*, 2011, 133, 10394-10397.
18 C. G. Zhang, Z. W. Peng, J. Lin, Y. Zhu, G. D. Ruan, C. C. Hwang, W. Lu, R. H. Hauge, J. M. Tour, *ACS Nano*, 2013, 7, 5151-5159.
19 C. S. Shan, W. J. Zhao, X. L. Lu, D. J. O'Brien, Y. P. Li, Z. Y. Cao, A. L. Elias, R. C. Silva, M. Terrones, B. Q. Wei, J. W. Suhr, *Nano Lett.*, 2013, 13, 5514-5520.
20 U. N. Maiti, W. J. Lee, J. M. Lee, Y. Oh, J. Y. Kim, J. E.Kim, J. Shim, T. H. Han, S. O. Kim, *Adv. Mater.*, 2014, 26, 40-67.
21 P. Chen, T. Y. Xiao, Y. H. Qian, S. S. Li, S. H. Yu, *Adv. Mater.*, 2013, 25, 3192-3196.
22 M. A. Mamo, A. O. Sustaita, Z. N. Tetana, N. J. Coville, I. A. Hümmelgen, *Nanotechnology*, 2013, 24, 125203.
23 Z. Gu, H. Peng, R. H. Hauge, R. E. Smalley, J. L. Margrave, *Nano Lett.*, 2002, 2, 1009-1013.
24 Y. Jiao, L. Zhang, X. R. Wang, G. Diankov, H. J. Dai, *Nature*, 2009, 458, 877-880.
25 R. P. B. dos Santos1, E. Perim, P. A. S. Autreto, G. Brunetto, D. S. Galv˜ao, *Nanotechnology*, 2012, 23, 465702.
26 H. W. Wang, Y. L. Wang, Z. G. Hu, X. F. Wang, *ACS Appl. Mater. Interfaces*, 2012, 4, 6827-6834.
27 N. Rubio, C. Fabbro, M. A. Herrero, A. de la Hoz, M. Meneghetti, J. L. G. Fierro, M. Prato, E. Vázquez, *Small*, 2011, 7, 665-674.
28 X. L. Li, H. L. Wang, J. T. Robinson, H. Sanchez, G. Diankov, H. J. Dai, *J. Am. Chem. Soc.*, 2009, 131, 15939-15944.
29 K. Xiao, Y. Q. Liu, P. A. Hu, G. Yu, Y. M. Sun, D. B. Zhu, *J. Am. Chem. Soc.*, 2005, 127, 8614-8617.
30 C. P. Ewels, M. Glerup, *J. Nanosci. Nanotechnol.*, 2005, 5, 1345-1363.
31 W. J. Zhang, J. Y. Zhang, P. J. Li, X. Shen, Q. F. Zhang, J. L. Wu, *Nanotechnology*, 2008, 19, 085202.
32 R. Czerw, M. Terrones, J. C. Charlier,| X. Blase, B. Foley, R. Kamalakaran, N. Grobert, H. Terrones, D. Tekleab, P. M. Ajayan, W. Blau, M. Ruhle, D. L. Carroll, *Nano Lett.*, 2001, 1, 457-460.
33 Y. Y. Shao, J. H. Sui, G. P. Yin, Y. Z. Gao, *Appl. Catal., B*, 2008, 79, 89-99.

34 Z. H. Sheng, L. Shao, J. J. Chen, W. J. Bao, F. B. Wang, X. H. Xia, *ACS Nano*, 2011, 5, 4350-4358.

35 Y Liu, Z. Jin, J. Y. Wang, R. L. Cui, H. Sun, F. Peng, L. Wei, Z. X. Wang, X. L. Liang, L. M. Peng, Yan Li, Adv. Funct. Mater., 2011, 21, 986-992.

36 D. S. Yu, Q. Zhang, L. M. Dai, *J. Am. Chem. Soc.*, 2010, 132, 15127-15129.

37 W. H. Shin, H. M. Jeong, B. G. Kim, J. K. Kang, J. W. Choi, *Nano Lett.*, 2012, 12, 2283-2288.

38 P. Ayala, R. Arenal, M. Rummeli, A. Rubio, T. Pichler, *Carbon*, 2010, 48, 575-586.

39 M.Terrones, *Nature*, 2009, 458, 845-846.

40 A. L. Higginbotham, D. V. Kosynkin, A. Sinitskii , Z. Z. Sun, J. M. Tour, *ACS Nano*, 2010, 4, 2059-2069.

41 W. S. Hummers, R. E. Offeman, J. Am. Chem. Soc. 1958, 80,1339–1339.

42 Z. Y. Lin, M. K. Song, Y. Ding, Y. Liu, M. L. Liu, C. P. Wong, *Phys. Chem. Chem. Phys.*, 2012, 14, 3381-3387.

43 T. Sharifi, E. Gracia-Espino, H. R. Barzegar, X. Jia, F. Nitze, G. Z. Hu, P. Nordblad, C. W. Tai, T. Wagberg, *Nat. Commun.*, 2013, 4, 2319.

44 Z. H. Sheng, L. Shao, J. J. Chen, W. J. Bao, F. B. Wang, X. H. Xia, *ACS Nano*, 2011, 5, 4350-4358.

45 J. R. Pels, F. Kapteijn, J. A. Moulijn, Q. Zhu and K. M. Thomas, *Carbon*, 1995, 33, 1641–1653.

46 I. Florea, O. Ersen, R. Arenal, D. Ihiawakrim, C. Messaoudi, K. Chizari, I. Janowska, C. P. Huu, *J. Am. Chem. Soc.*, 2012, 134,9672-9680.

47 L. Sun, C. G. Tian, Y. Fu, Y. Yang, J. Yin, L. Wang, H. G. Fu, *Chem. Eur. J.*, 2014, 20, 564-574.

48 S. Lim, S. Yoon, I. Mochida, D. Jung, *Langmuir*, 2009, 25, 8268-8273.

49 Y. S. Yun, H. H. Park, H. J. Jin, *Material*, 2012, 5, 1258-1266.

50 D. D. Zhou, W. Y. Li, X. L. Dong, Y. G. Wang, C. X. Wang, Y. Y. Xia, *J. Mater.Chem. A*, 2013, 1, 8488– 8496.

51 L. C. Li, Y. C. Liu, X. Geng, B. G. An, *Adv. Mater. Res.*, 2011, 160-162, 1791-1976.

52 L. Sun, L. Wang, C. G. Tian, T. X. Tan, Y. Xie, K. Y. Shi, M. T. Li, H. G. Fu, *RSC Adv.*, 2012, 2, 4498-4506.

53 R. Kötza, M. Carlenb, *Electrochim. Acta*, 2000, 45, 2483-2498.

54 H. L. Guo, P. Su, X. F. Kang, S. K Ning, *J. Mater.Chem. A*, 2013, 1, 2248-2255.

55 L. F. Lai, J. R. Potts, D. Zhan, L. Wang, C. K. Poh, C. H. Tang, H. Gong,d Z. X. Shen, J. Y. Lin, R. S. Ruoff, *Energy Environ. Sci.*, 2012, 5, 7936-7942.

56 N. P. Subramanian, X. G. Li, V. Nallathambi, S. P. Kumaraguru, H. C. Mercado, G. Wu, J. W. Lee, B. N. Popov, *J. Power Sources*, 2009, 188, 38-44.